ACS APPLIED MATERIALS & INTERFACES

Research Article

www.acsami.org

High-Efficiency Photoelectrochemical Properties by a Highly Crystalline CdS-Sensitized ZnO Nanorod Array

Yuyu Bu,[†] Zhuoyuan Chen,*[,†] Weibing Li,[‡] and Jianqiang Yu[§]

[†]Key Laboratory of Marine Environmental Corrosion and Bio-fouling, Institute of Oceanology, Chinese Academy of Sciences, 7 Nanhai Road, Qingdao 266071, China

[‡]School of Environment and Safety Engineering, Qingdao University of Science and Technology, 53 Zhengzhou Road, Qingdao 266042, China

[§]Key Laboratory of New Fiber Materials and Modern Textile, Qingdao University, 308 Ningxia Road, Qingdao 266071, China

ABSTRACT: A ZnO nanorod array with comparatively long nanorods was successfully prepared on a Ti substrate by applying a hydrothermal method twice. CdS nanoparticles with high crystallinity were deposited onto the surface of ZnO nanorods through a galvanostatic electrodeposition method. CdS-sensitized ZnO nanorod arrays after being hydrothermally grown twice with the second growth time of 6 h possessed the best photoelectrochemical performance. The photoinduced current densities at a 0 V bias potential are 23.7 and 15.8 mA·cm^{-2} under the illumination of simulated sunlight and visible light, respectively. The monochromatic incident photon-to-electron conversion efficiency values at the wavelength of 380–520 nm are in the range of 50–60%, which indicated its high photoelectric conversion efficiency. The contribution from visible light is significantly higher than that from UV light. The prepared photoanodes in the present work exhibit a potential application in photoelectrochemical hydrogen production from water reduction under sunlight.

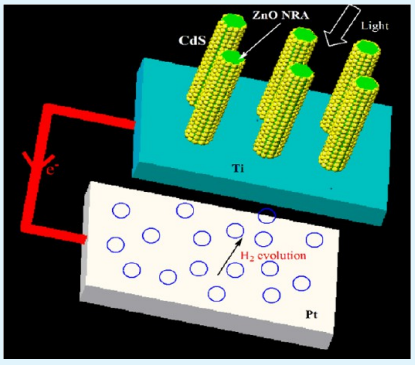

KEYWORDS: *ZnO nanorod array, CdS quantum dot, photoelectrochemical performance, visible light illumination*

1. INTRODUCTION

Zinc oxide (ZnO) is a semiconductor material with a wide bandgap that exhibits excellent photoelectrochemical performance. This material has been extensively studied in photoelectrochemical hydrogen production from water splitting,[1−4] photocatalytic degradation of organic pollutants,[5−8] dye-sensitized solar cells,[9−12] photoluminescence materials,[13,14] gas sensing,[15,16] etc. Compared with TiO_2, which was the first semiconductor material applied in photoelectric conversion, ZnO is both environment-friendly and inexpensive. In addition, electron mobility in ZnO is approximately two orders of magnitude higher than that in TiO_2. This higher electron mobility can effectively improve the migration rate of photogenerated electrons in ZnO to inhibit the recombination of photogenerated electrons and holes.[17] Thus, ZnO is considered a photovoltaic semiconductor material with significant application potential.

Narrow band gap quantum dots sensitized with one-dimensional TiO_2 and ZnO nanotube,[18−22] nanorod,[23−27] nanobelt[28−30] arrays and nanoplate[31,32] structures have recently been widely used in photoelectrochemical hydrogen production from water reduction. These semiconductor materials with one-dimensional ordered nanostructure have significantly better properties compared with disordered semiconductor nanoparticle film structures. Nanostructure semiconductor materials grown perpendicular to the conductive substrate can streamline the delivery path of photogenerated electrons, thereby effectively reducing the recombination probability of photogenerated electrons and holes. Moreover, these nanostructures have a large specific surface area, which could provide a large number of loading sites for other semiconductor materials that respond to visible light.

Ye et al[33] prepared a TiO_2 nanotube array on a Ti substrate using an electrochemical multianodized method and then modified the material through Pd nanoparticle loading. Under a Xe light source (320 mW·cm^{-2}), the photogenerated current density was 26 mA·cm^{-2} at an applied bias of 1.0 V (vs Ag/AgCl) with glycol as hole scavengers. Paulose et al.[34] prepared a 45 μm long TiO_2 nanotube array using an anodic oxidation method. Under UV light (95 mW·cm^{-2}), the photogenerated current density was 26 mA·cm^{-2} at an applied bias of 1.0 V (vs Ag/AgCl) in a KOH solution.

Although the aforementioned semiconductor materials have relatively high hydrogen production photoelectrochemical properties from water splitting, these materials only respond to UV light, the energy of which accounts for only 4% of the solar spectrum.[35] Thus, these materials are mismatched with the solar spectrum, because of which they cannot use solar energy effectively. Therefore, semiconductor materials that respond to visible light with high efficiency must be developed to facilitate further application of this technology.

Received: March 16, 2013
Accepted: May 20, 2013
Published: May 20, 2013

Wang et al.[23] prepared TiO_2 nanorod arrays (NRAs) grown perpendicular to an F-doped SnO_2 conductive glass using a hydrothermal method. The material was then sensitized with CdS quantum dots using a chemical bath deposition method. Under a 100 mW·cm^{-2} AM 1.5 G light source, the photogenerated current density was 5.777 mA·cm^{-2} in a polysulfide solution at an applied bias of 0 V (vs Ag/AgCl). Seol et al.[28] prepared ZnO nanowire arrays that were jointly sensitized with CdSe and CdS quantum dots. The photogenerated current density was 9.15 mA·cm^{-2} under the same test conditions as Wang et al.[23] The increase in photogenerated current density was attributed to the wide optical absorption range of the CdSe quantum dots and to the band potential difference between CdSe and CdS. These characteristics enhanced the separation efficiency of the photogenerated electron−hole pairs. Wang et al.[29] prepared ZnO NRAs on both sides of an indium tin-oxide conductive glass, which were sensitized with CdS and CdSe. The results showed that photoelectric conversion efficiency improved significantly compared with that of one-sided photoanode.

In this work, the authors prepared a ZnO NRA with relatively long nanorods on a Ti plate substrate by applying a hydrothermal method twice. Ti substrate was selected for two reasons. First, Ti substrate has low work function, which can reduce the energy barrier of the photogenerated electron transfer from the ZnO nanorods to the Ti substrate. Second, a dense layer of oxide film forms on a Ti substrate during processing. This film can effectively suppress dark current losses. Subsequently, CdS nanoparticles with comparatively high crystallinity were deposited onto the ZnO nanorod surfaces using a galvanostatic electrodeposition method. The photoelectrochemical performance of this material was mainly studied under visible light.

2. EXPERIMENTAL SECTION

2.1. Preparation of ZnO NRA. The ZnO NRA preparation on the Ti substrate was primarily based on the method used by Law et al.[9] with minor modifications. First, a ZnO nanoparticle seed layer was deposited onto the Ti substrate (>99.6% purity; 5 cm × 1 cm) by applying the following steps: Concentrations of 0.01 mol zinc acetate and 0.012 mol diethanolamine were dissolved in 25 mL anhydrous alcohol. A homogeneous sol was formed after 30 min of stirring at 60 °C. An even sol film was formed on the Ti substrate by using a dip-coating method (1 cm·min^{-1} pulling rate). A uniform ZnO nanoparticle seed layer was formed after heating the sol film at 500 °C for 10 min. A total volume of 100 mL mixed solution containing 2.5 mmol zinc acetate, 2.5 mmol hexamethylenetetramine, and 0.6 mmol polyethyleneimine was then prepared and stirred for 20 min in an ice bath. Subsequently, 80 mL of the mixed solution was transferred to a polytetrafluoroethylene tube with a total volume of 100 mL. The Ti plate prepared with a ZnO nanoparticle seed layer was immersed into the solution and faced down, maintained at a certain angle versus the tube wall, and hydrothermally reacted for 4 h at 95 °C. The prepared sample was repeatedly rinsed with deionized water and anhydrous alcohol, after which it was annealed at 500 °C for 1 h. The hydrothermal reaction was repeated one more time to increase the length of the ZnO nanorods. The second reaction duration was controlled at 2, 4, 6, and 8 h, respectively. All reagents used in this study were analytical ones from Aladin Industrial Corporation, China.

2.2. Preparation of CdS-Sensitized ZnO NRA Photoanodes. The CdS-sensitized ZnO NRA photoanode was prepared through the following steps: CdS nanoparticles were galvanostatically electrodeposited onto the ZnO NRA surfaces (the exposed geometric area is 1 cm × 1 cm). The electrolyte for electrodeposition was a mixture of 0.2 mol·L^{-1} cadmium nitrate, 0.2 mol·L^{-1} thiourea, 25 mL dimethylsulfoxide, and 25 mL deionized water. The ZnO NRA acted as the working electrode, and a platinum sheet acted as the counter electrode. The electrodeposition current density was 0.5 mA·cm^{-2}, and the electrodeposition temperature was 90 °C. The electrodeposition time was 30 min. The sample was then repeatedly rinsed with deionized water and anhydrous alcohol. Finally, the sample was dried at 80 °C for 2 h in vacuum.

2.3. Characterizations of ZnO NRA and CdS-Sensitized ZnO NRA. The morphologies and the elemental compositions of the prepared photoelectrodes were analyzed using a scanning electron microscope (SEM) (JSM-6700F; JEOL, Tokyo, Japan) with an energy dispersive spectrometer (EDS) (INCA Energy, Oxford). The crystalline structures of the photoelectrodes were identified through X-ray diffraction (XRD) (D/MAX-2500/PC; Rigaku Co., Tokyo, Japan). The CdS distribution onto the ZnO nanorod surfaces, and the CdS/ZnO interface bonding information was analyzed using a high-resolution transmission electron microscope (HRTEM, FEI Tecnai G20). The optical absorption properties of the photoelectrodes were investigated using a UV/vis diffuse reflectance spectrophotometer (U-41000; HITACHI, Tokyo, Japan).

2.4. Photoelectrochemical Measurements. A three-electrode system was employed to measure the photoinduced volt−ampere characteristic curve (I−V curve) and the varations of the photoinduced current density with time (i−t curve) of the prepared photoelectrodes using the CHI660D Electrochemical Workstation (Shanghai Chenhua Instrument Co., Ltd., Shanghai, China). The photoelectrodes (1 cm × 1 cm), Ag/AgCl, and platinum electrode acted as the working, reference and counter electrodes, respectively. The electrolyte was 0.25 mol·L^{-1} Na_2S + 0.35 mol·L^{-1} Na_2SO_3. The I−V curves were measured from −1.5 to 1.0 V with a scan rate of 0.05 V·s^{-1}. The gap between the switching on and turning off of the light was 1 s. The i−t curves were measured at a 0 V bias potential. The white light source was a 150 W Xe arc lamp (PLS-SXE300, Beijing Changtuo Co. Ltd., Beijing, China) with an optical intensity of 265 mW·cm^{-2}. A 420 nm cutoff filter was used to remove light with wavelengths less than 420 nm, ultimately generating visible light with an optical intensity of 200 mW·cm^{-2}. The photoelectric conversion efficiency of the photoelectrodes was studied based on their monochromatic incident photon-to-electron conversion efficiency (IPCE) spectra, which were measured using a 500 W Xe lamp with a monochromator. The light-sensing surface area was 0.5 cm × 0.5 cm.

3. RESULTS AND DISCUSSION

3.1. Surface Texture of ZnO NRA and CdS-Sensitized ZnO NRA Photoelectrodes. Figure 1 shows the SEM images of the ZnO NRA after being hydrothermally grown once (Figure 1a) and twice (Figures 1b−e) as well as the SEM image (Figure 1f) and EDS (Figure 1g) of the CdS-sensitized ZnO NRA thin-film photoelectrode. The growth time of the second hydrothermal reaction was controlled at 2 (Figure 1b), 4 (Figure 1c), 6 (Figure 1d), and 8 h (Figure 1e). Figure 1a shows the cross-section morphology of the ZnO NRA after being hydrothermally grown once. The ZnO nanorods were grown evenly on the seed layer, and the rod length was approximately 1 μm. Figure 1b shows the morphology of the ZnO NRA after being hydrothermally grown twice, with a second reaction time of 2 h. Compared with Figure 1a, the ZnO nanorod length did not increase significantly, which can be attributed to the fact that the ZnO nanorods did not exhibit uniform growth during the whole hydrothermal reaction process, but initially underwent a slow growth period before entering a rapid growth stage.

Prolonging the second reaction time to 4 h (Figure 1c) resulted in a rapid increase in the ZnO nanorod length to 4 μm, which indicates that the ZnO NRA entered a rapid growth stage after 2 h of the second hydrothermal reaction. Figure 1d shows the morphology of the ZnO NRA after 6 h of the second hydrothermal reaction. The ZnO nanorod length increased to

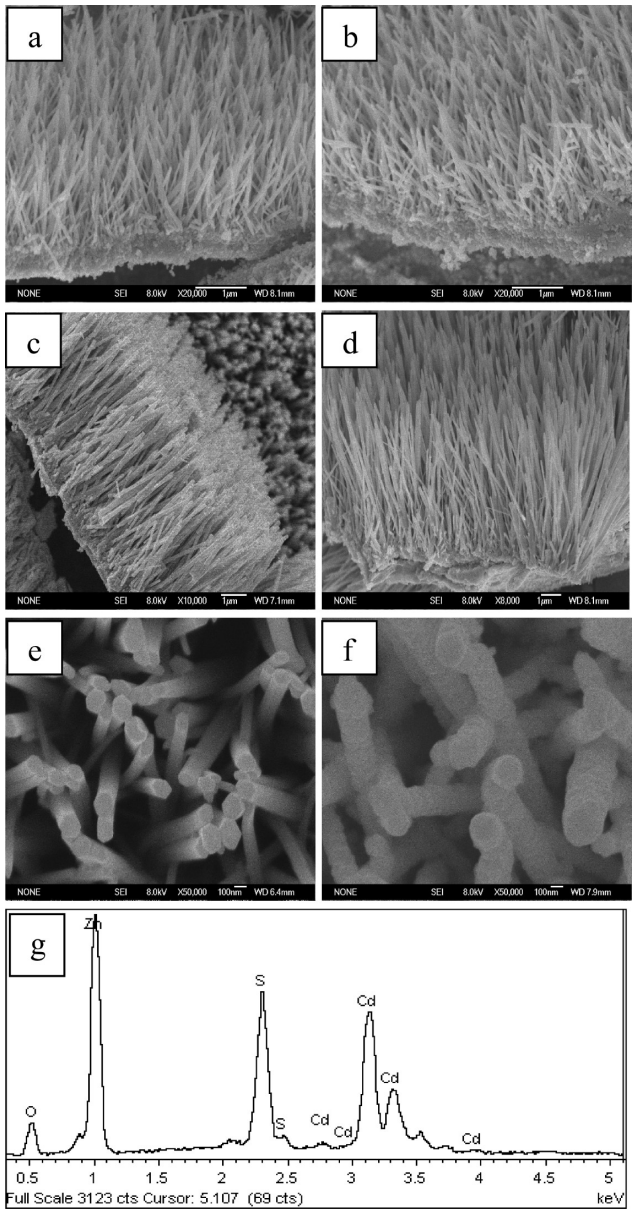

Figure 1. SEM images of the ZnO NRA after being hydrothermally grown once (a) and twice (b–e) as well as the SEM image (f) and EDS (g) of the CdS-sensitized ZnO NRA thin-film photoelectrode. The growth time of the second hydrothermal reaction was controlled at 2 (b), 4 (c), 6 (d), and 8 h (e).

approximately 7 μm but did not exhibit a significant increase after >6 h of the second hydrothermal reaction. Longer nanorods could provide a larger number of loading sites for CdS deposition.

Figure 1e shows the morphology of the ZnO NRA under higher magnification than that in Figure 1d. The nanorod diameter is approximately 100 nm, and the rod exhibited a regular hexagonal growth. Figure 1f shows the morphology of the CdS-sensitized ZnO NRA under higher magnification after 6 h of the second hydrothermal growth. As shown in Figure 1f, CdS was evenly deposited onto the ZnO nanorod surface and the diameter of the rods increased to approximately 200 nm. Thus, the CdS deposition thickness was approximately 50 nm. Figure 1g shows the EDS results of the CdS-sensitized ZnO NRA shown in Figure 1f. Only Zn, O, Cd, and S elements were observed, revealing that only Cd- and S-containing substances were deposited onto the ZnO surface. Combined with the XRD results shown in the following section, the substance deposited onto the ZnO surface can be identified as CdS. In addition, the atomic percentages of Cd and S were relatively high based on the EDS results, indicating that a large amount of CdS was deposited onto the ZnO surface.

3.2. TEM Information. Figure 2 shows the HRTEM morphologies of the CdS-sensitized ZnO NRA after 6 h of the second hydrothermal growth. Figure 2a shows the microscopic morphology under low magnification. Although a brittle fracture of the ZnO nanorods occurred during the splitting of the nanorods from the Ti substrate and their subsequent dispersion into anhydrous ethanol, the CdS nanoparticles were observed to be evenly distributed onto the ZnO nanorod surface. Figure 2b shows the microscopic morphology under

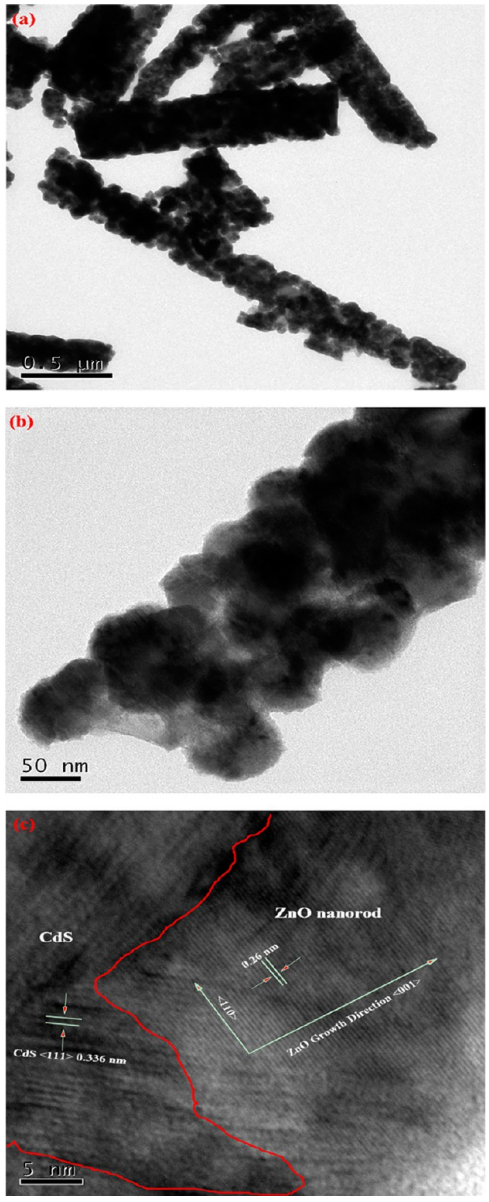

Figure 2. HRTEM morphologies of the CdS-sensitized ZnO NRA after being hydrothermally grown twice with the second growth time of 6 h.

dx.doi.org/10.1021/am400964c | ACS Appl. Mater. Interfaces 2013, 5, 5097–5104

medium magnification. The CdS nanoparticles with diameters of approximately 50 nm homogeneously covered the surface of the ZnO nanorods in nearly a single layer. Thus, the diameter of the nanorods increased to approximately 200 nm. This result is in agreement with that shown in Figure 1f. Figure 2c shows the HRTEM image of the CdS/ZnO interface under high magnification. According to Greene et al.,[36] ZnO nanorods prepared by applying a hydrothermal method gradually grow along the (001) crystal plane. Figure 2c clearly shows the ZnO (001) crystal plane with a width of approximately 0.26 nm. This value corresponds to the standard lattice parameters from the XRD. On the ZnO surface, the CdS (111) crystal plane was observed with a width of approximately 0.336 nm. The crystal interface between ZnO and CdS was closely combined, thus enabling the CdS photogenerated electrons to transfer swiftly onto the ZnO and consequently inhibiting the recombination of the photogenerated electrons and holes effectively.

3.3. Crystal Structure of ZnO NRA and CdS-Sensitized ZnO NRA. Figure 3 shows the XRD patterns of the ZnO NRA and CdS-sensitized ZnO NRA. The crystal structure of the ZnO nanorod is similar to that of a wurtzite. A high-intensity diffraction peak was observed in the ZnO (002) crystal plane, revealing that the ZnO nanorod was grown in a highly ordered manner along the ⟨001⟩ direction. The CdS diffraction peaks indicated that CdS existed on the ZnO surface in a cubic structure, and the higher peak intensities of the CdS diffraction peaks indicated a comparatively high crystallinity of the electrodeposited CdS.

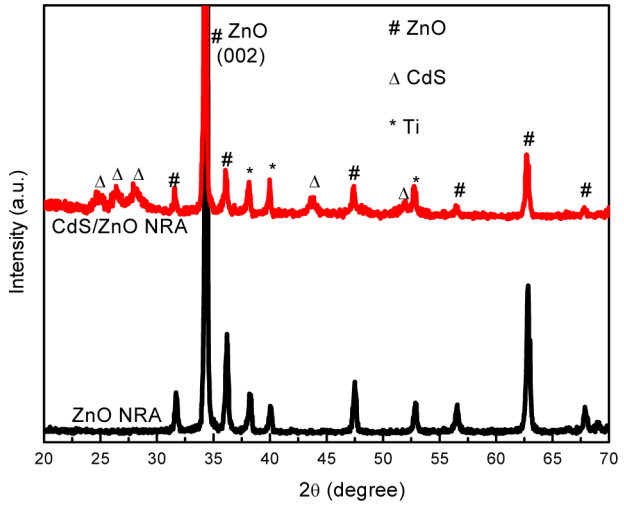

Figure 3. XRD patterns of the ZnO NRA and CdS-sensitized ZnO NRA.

3.4. Photoelectrochemical Performance. The photoelectrochemical performance of the ZnO NRA and CdS-sensitized ZnO NRA photoelectrodes was studied using the *i*−*t* and *I*−*V* curves. Figure 4 shows the *i*−*t* curves obtained at a 0 V bias potential under white light. Curve 4a shows that the photoinduced current density of the ZnO NRA that was hydrothermally grown once is 1.4 mA·cm^{-2}. However, the photoinduced current density of the ZnO NRA after 6 h of the second hydrothermal growth increased to 4.0 mA·cm^{-2}, as shown in curve 4b. These results can primarily be attributed to the fact that longer ZnO nanorods have a larger specific area, thus providing more sites for photoelectrochemical reactions and enhancing the photoinduced current density.

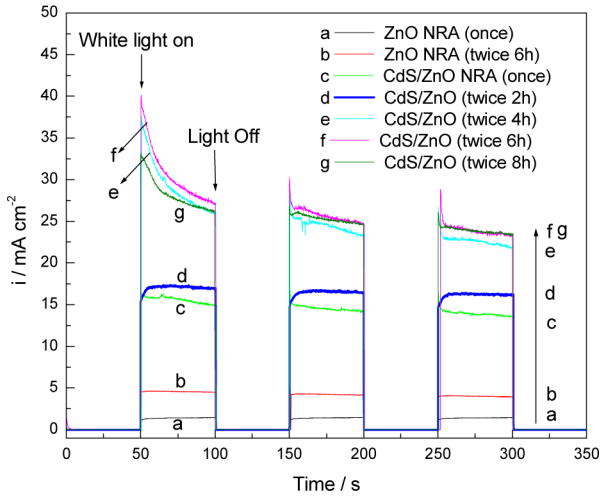

Figure 4. Varations of the photoinduced current density with time of ZnO NRA after being hydrothermally grown once (curve a) and twice with the second growth time of 6 h (curve b); CdS-sensitized ZnO NRA after being hydrothermally grown once (curve c) and twice with a second growth time of 2 (curve d), 4 (curve e), 6 (curve f) and 8 h (curve g), respectively. All curves were obtained at 0 V bias potential under white light on and off.

Curve 4c is the *i*−*t* curve of the CdS-sensitized ZnO NRA. ZnO was hydrothermally grown once. The photoinduced current density increased to 14.0 mA·cm^{-2}, a value that is approximately 10 times greater than that of ZnO NRA hydrothermally grown once without CdS sensitization. This result can be attributed to the broadening of the light absorption range by CdS and to the promotion of the separation efficiency of the photogenerated electron−hole pairs by the formation of the interface electric field in the CdS/ZnO interface. Curves 4d−g show the *i*−*t* curves of the series of CdS-sensitized ZnO NRAs that were hydrothermally grown twice with the second growth time of 2 (curve 4d), 4 (curve 4e), 6 (curve 4f), and 8 h (curve 4g), respectively. The photoinduced current density significantly increased from 16.1 mA·cm^{-2} to 22.3 mA·cm^{-2} as the second hydrothermal growth time increased from 2 to 4 h. When the second hydrothermal growth time was increased to 6 and 8 h, the photoinduced current density did not exhibit a significant increase, eventually stabilizing at approximately 23.7 mA·cm^{-2}. These results indicate that the ZnO nanorods underwent a slow crystal growth process at the initial 2 h of the second hydrothermal reaction. Thereafter, the crystal growth accelerated, thus facilitating a rapid increase in the length and specific area of the nanorods. After the second hydrothermal growth time was increased to 6 h, the nanorod lengths reached the maximum values, thus stabilizing the specific area. This behavior was reflected in the gradual stabilization of the photoinduced current density.

Figure 5 shows the *I*−*V* curves of the CdS-sensitized ZnO NRA after being hydrothermally grown once (curve 5a) and twice with the second growth time of 6 h (curve 5b) under white light. For the CdS-sensitized ZnO NRA that was hydrothermally grown once, an anodic current was generated at a −1.4 V bias potential, slowly increasing with the positive shift of the potential. After the bias potential reached −0.4 V, the current became more stable. When the bias potential increased to 1.0 V, the photoinduced current density was 15.9 mA·cm^{-2}. For the CdS-sensitized ZnO NRA after being

dx.doi.org/10.1021/am400964c | ACS Appl. Mater. Interfaces 2013, 5, 5097−5104

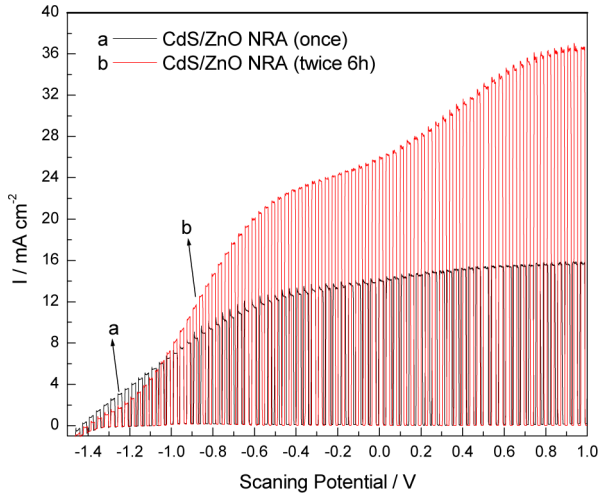

Figure 5. Photoinduced volt−ampere characteristic curves of the CdS-sensitized ZnO NRA after being hydrothermally grown once (curve a) and twice with the second growth time of 6 h (curve b) under white light.

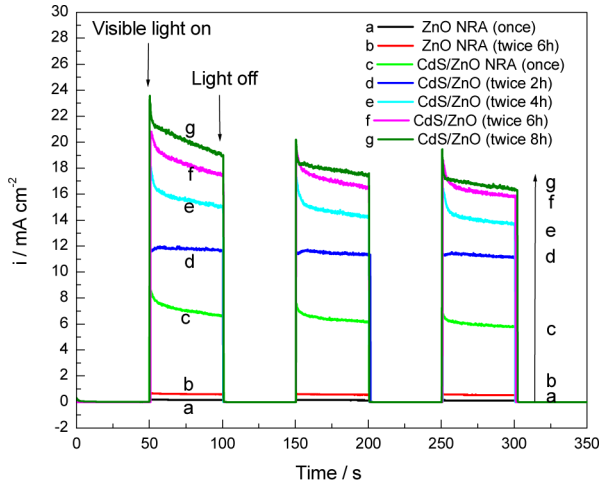

Figure 6. Varations of the photoinduced current density with time of ZnO NRA after being hydrothermally grown once (a) and twice with the second growth time of 6 h (b); CdS-sensitized ZnO NRA after being hydrothermally grown once (c) and twice with the second growth time of 2 (d), 4 (e), 6 (f), and 8 h (g). All curves were obtained at 0 V bias potential under visible light on and off.

hydrothermally grown twice, the current slowly increased in the −1.4 to −1.2 V bias potential range. The current density surpassed that generated from the former photoanode at a −1.05 V bias potential. After the bias potential reached > −1.2 V, the current density increased rapidly. When the bias potential increased to 1.0 V, the photoinduced current density increased to 36.6 mA·cm^{-2}. At this point, the bubbles generated by hydrogen evolution continuously welled up, indicating the very strong hydrogen production capacity resulting from the water reduction of this photoelectrode.

Under white light, the CdS-sensitized ZnO NRA, after being hydrothermally grown twice with the second growth time of 6 h, achieved an extremely high photoelectrochemical hydrogen production performance. However, the photoelectrochemical hydrogen production performance of the series of CdS-sensitized ZnO NRA photoelectrodes must be verified under visible light for efficient solar energy utilization. Figure 6 shows the *i*−*t* curves obtained at a 0 V bias potential under visible light. For the photoelectrodes without CdS, a negligible photoinduced current was generated, as shown in curves 6a and b. The ZnO absorption wavelengths are known to be below 380 nm;[5] this characteristic was proven by the subsequent UV/vis results. Thus, ZnO cannot absorb visible light. This small photogenerated current density, as shown in curves 6a and b, may be attributed to the inevitable faint UV light leakage from the light filter. The photoinduced current density of the CdS-sensitized ZnO NRA that was hydrothermally grown once reached 5.8 mA·cm^{-2}, only 41.4% of that under white light. However, the photoinduced current densities of the CdS-sensitized ZnO NRA after being hydrothermally grown twice with the second growth time of 2, 4, 6, and 8 h are 11.2, 13.7, 15.8, and 16.3 mA·cm^{-2}, respectively. All the decreasing amplitudes were <40% of that under white light. These results reveal that the ZnO NRA that was hydrothermally grown twice can provide more loading sites for CdS nanoparticles than hydrothermally grown only once. Therefore, the visible light absorption of the former photoelectrodes is more complete than that of the latter. The photoelectrodes can thus generate high current density after UV light filtration. This result indicates that the majority of the photogenerated current was contributed by the visible light absorption of the photoanodes.

Figure 7 shows the *I*−*V* curves of the ZnO NRA after being hydrothermally grown twice with the second growth time of 6

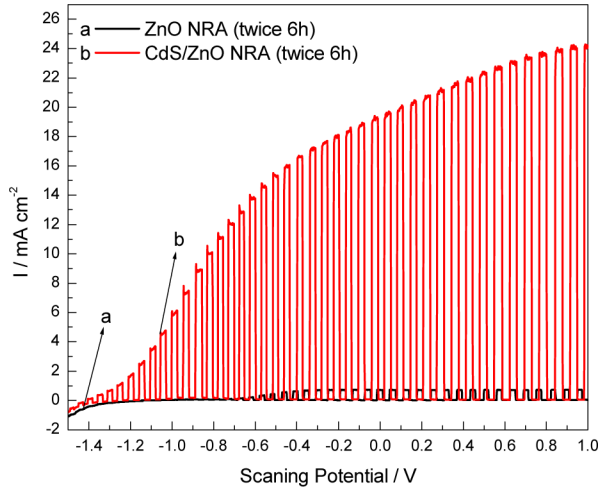

Figure 7. Photoinduced volt−ampere characteristic curves of the ZnO NRA after being hydrothermally grown twice with the second growth time of 6 h without (a) and with (b) CdS quantum dots under visible light.

h without (a) and with (b) CdS nanoparticles under visible light. For the ZnO NRA, a faint current density was generated at a −0.6 V bias potential, remaining at a weak level up to a 1.0 V bias potential. As previously mentioned, this result could be attributed to the faint UV light leakage from the light filter. However, the CdS-sensitized ZnO NRA generated a photoinduced current density from a −1.4 V bias potential, and the values increased with the positive scan of the bias potential. The photoinduced current density was 24.2 mA·cm^{-2} at a 1.0 V bias potential, 66.1% of that at the same condition under white light. The results likewise indicate that the photoinduced current density is primarily contributed by visible light rather than UV

dx.doi.org/10.1021/am400964c | ACS Appl. Mater. Interfaces 2013, 5, 5097−5104

light absorption. Therefore, this photoanode can effectively match the actual solar spectrum.

Figure 8 shows the UV/vis diffuse reflectance spectra of the ZnO NRA without (curves a and b) and with (curves c and d)

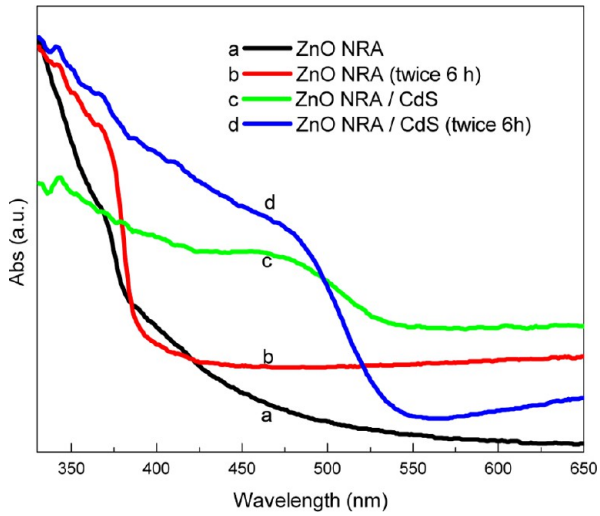

Figure 8. UV/vis diffuse reflectance spectra of the ZnO NRA without (curves a and b) and with (curves c and d) CdS quantum dots. The ZnO NRA was hydrothermally grown once (curves a and c) and twice with the second growth time of 6 h (curves b and d).

CdS nanoparticles. The ZnO NRA was hydrothermally grown once (curves a and c) and twice after 6 h of the second hydrothermal growth (curves b and d). The ZnO NRA without CdS exhibited absorption primarily in the UV region, and the light absorption threshold was approximately 380 nm, which corresponds to the standard absorption range of ZnO.[5] Comparing the UV/vis diffuse reflectance spectra, the optical absorption intensity of the ZnO NRA that was hydrothermally grown twice is evidently larger than that hydrothermally grown only once, illustrating that a longer rod body structure is conducive to the improvement of photon capture efficiency. After being sensitized by the CdS nanoparticles, the optical absorption range of the materials extended to the visible light region, and the light absorption threshold was approximately 540 nm. The optical absorption capacity of the CdS-sensitized ZnO NRA that was hydrothermally grown twice is evidently stronger than that of the CdS-sensitized ZnO NRA hydrothermally grown once in both the visible light and UV regions.

Although UV/vis diffuse reflectance spectroscopy can be used to characterize the absorption capacity of the photons of the above photoelectrodes at different wavelengths, this approach cannot strictly characterize the photoelectric conversion efficiency of these photoelectrodes. Photons are not completely converted into available electrons after absorption. A number of photogenerated electrons would recombine with holes and then be converted to heat, resulting in energy dissipation. Thus, the monochromatic incident photon-to-electron conversion efficiency (IPCE) spectra for the photoelectrodes were measured to characterize photoelectric conversion efficiency. The results are shown in Figure 9.

The IPCE curves were drawn by measuring the photogenerated current density i_m (μA·cm^{-2}) under monochromatic incident light with an intensity of P_m (W·m^{-2}). The IPCE values (%) can be calculated according to the following formula:

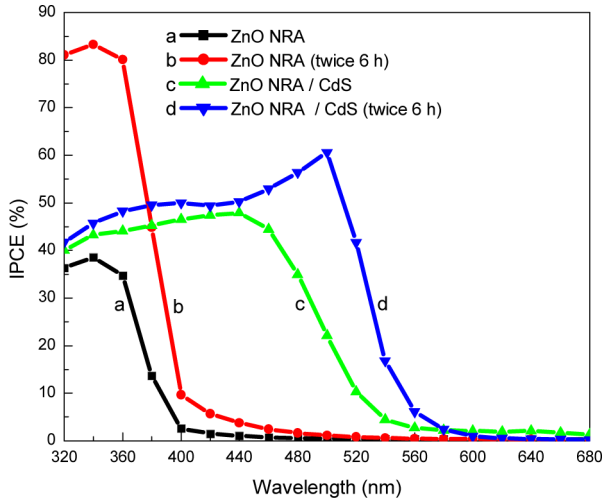

Figure 9. Monochromatic incident photon-to-electron conversion efficiency (IPCE) spectra of ZnO NRA without (a and b) and with (c and d) CdS quantum dots. The ZnO NRA was hydrothermally grown once (a and c) and twice with the second growth time of 6 h (b and d).

$$\mathrm{IPCE}(\%) = \frac{1240 i_m}{\lambda P_m} \quad (1)$$

Comparing the IPCE curves of the ZnO NRAs that were hydrothermally grown once (curve 9a) and twice (curve 9b), the photoelectric conversion efficiency of the former is observed to be significantly lower than that of the latter. The photoelectric conversion efficiency of the latter is more than 80% in the 320−360 nm wavelength. These results correspond to the photoinduced current density shown in Figure 4. In Figure 4, the photoinduced current density of the ZnO NRA that was hydrothermally grown twice is approximately three times greater than that was hydrothermally grown once. After sensitization with CdS, the IPCE values decreased to approximately 40−50% of those of the ZnO NRA after being hydrothermally grown twice with the second growth time of 6 h in the wavelength range of 320−360 nm. These results revealed that CdS was the main photoabsorption material after loading with CdS and the ZnO NRA played the role of transferring of the photogenerated electrons at this situation. Therefore, the absorption capacity of CdS is lower than that of ZnO NRA in the ultraviolet region. The photoelectric conversion efficiency of the ZnO NRA that was hydrothermally grown twice is higher than that hydrothermally grown once in the whole absorption region, as shown in Figure 9. The photoelectric conversion efficiency of the ZnO NRA hydrothermally grown once sharply decreased when the incident wavelength was larger than 440 nm. However, the photoelectric conversion efficiency of the ZnO NRA hydrothermally grown twice increased with the incident wavelength when such a wavelength was larger than 440 nm. After the wavelength increased to 520 nm, the photoelectric conversion efficiency sharply decreased. The photoelectric conversion efficiency of the ZnO NRA hydrothermally grown twice was greater than 50% when the wavelength was larger than 380 nm, and this value increased to 60% and higher when the wavelength was at 520 nm. These results are significantly higher than those obtained by Wang et al.,[23] that is, 20% for the CdS-sensitized TiO_2 NRA and those of Wang et al.[29] were 45% for the CdS and CdSe jointly sensitized ZnO NRA. The high photoelectric

conversion efficiency of the CdS-sensitized ZnO NRA after being hydrothermally grown twice with the second growth time of 6 h in the visible region is the main reason for its large photogenerated current density under visible light.

Although the CdS-sensitized ZnO NRA after being hydrothermally grown twice with a second reaction time of 6 h possesses very high photoelectrochemical performance under visible light, the stability of this photoelectrode is required to further study in order to apply this material to the area of the photoelectrochemical hydrogen production from water splitting. Figure 10 shows the variations of the photoinduced

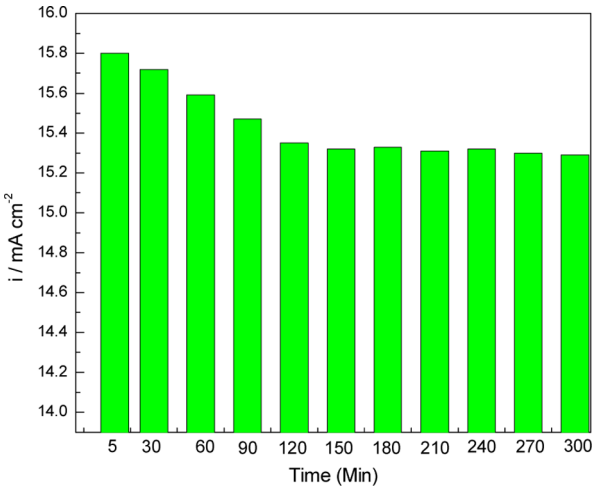

Figure 10. Photoelectrochemical stability of the CdS-sensitized ZnO NRA after being hydrothermally grown twice with a second reaction time of 6 h under visible light illumination.

current density of the CdS-sensitized ZnO NRA after being hydrothermally grown twice with a second reaction time of 6 h under 5 h visible light illumination. As the results showed in Figure 10, the photogenerated current density is 15.8 mA·cm^{-2} after 5 min of visible light illumination, and it decreases with the increase of illumination duration. After the illumination time increases to 120 min, the photogenerated current density decreases to approximately 15.3 mA·cm^{-2} and stabilizes at this value after longer illumination, which exhibits its high stability. This can be caused by the diffusion of the polysulfide electrolyte, which is a hole scavenger. The polysulfide electrolyte is completely adsorbed on the photoelectrode surface at the beginning of the light illumination, and this electrolyte can rapidly capture the photogenerated holes by CdS and hence generate larger photoinduced current. With the prolongation of the illumination, the polysulfide electrolyte is gradually oxidized due to the reaction with the photogenerated holes and the concentration of the polysulfide adsorbed on the electrode surface decreases. The electrochemical reactions are controlled by the concentration polarization and, thus, results in the decrease of the photoinduced current. After the concentration diffusion achieved to be stable, the photogenerated current reached a stable value, as showed in Figure 10.

Figure 11 schematically shows the significant promotion principles of the photoelectrochemical performance of the CdS-sensitized ZnO NRA after being hydrothermally grown twice on a Ti substrate. The ZnO nanorod surface grown on the Ti substrate was evenly covered by a single layer of CdS nanoparticles with relatively large particle sizes. Under visible

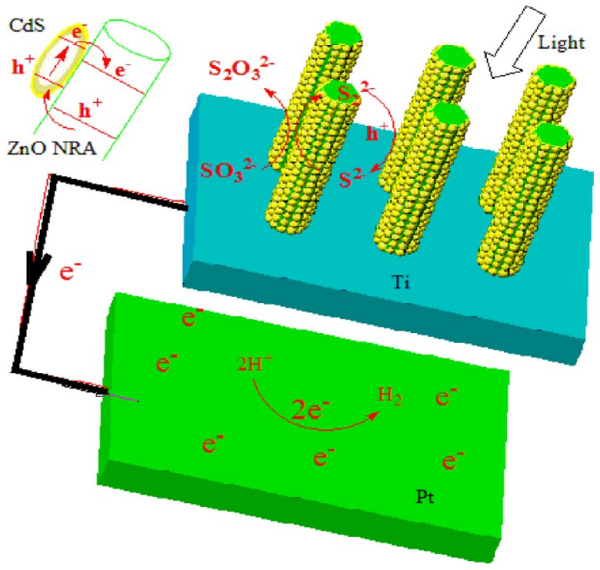

Figure 11. Schematically illustration of the significant promotion principles of the photoelectrochemical performance of the CdS-sensitized ZnO NRA after being hydrothermally grown twice on Ti substrate.

light, the photovoltaic effect of CdS resulted in the generation of electrons and holes. The conduction band potential of CdS is more negative than that of ZnO. The photogenerated electrons can flow from the conduction band of CdS into that of ZnO. Finally, the electrons can transfer to the Pt counter electrode, flowing through the ZnO nanorod body, Ti substrate, and copper wire. The electrons on the Pt electrode surface then react with water to generate hydrogen. Moreover, the photogenerated holes transfer to the CdS surface and are then captured by the surrounding polysulfide electrolyte. Emin el al.[31] detailedly discussed the reaction processes of the photogenerated holes on the surface of CdS. The ZnO nanorods after being hydrothermally grown twice are longer than those after being hydrothermally grown only once. Longer nanorods could provide more deposition sites for CdS nanoparticles. The CdS nanoparticles prepared in this work possess comparatively high crystallinity, thus facilitating the transfer of electrons in CdS. The diameters of the CdS prepared in this work are approximately 50 nm, and the CdS are evenly distributed onto the ZnO nanorod surface as a single and compact layer. This thick CdS film provides a thick depletion layer. Therefore, a more powerful n−n junction electric field was formed between CdS and ZnO, improving the transfer capacity of the photogenerated electrons and holes on the interface. The tight coverage of the CdS on the ZnO surface could reduce the ZnO area that is directly exposed to the electrolyte, effectively inhibiting the photogenerated electrons transferred to ZnO from reacting with the oxidizing substances in the electrolyte and from being consumed as a dark current. Finally, compared with the CdS quantum dot nanolayer, the single layer of larger CdS nanoparticles significantly reduced the migration path of the photogenerated electrons and prevented the energy loss resulting from the migration of the photogenerated electrons between the CdS nanoparticles. On the basis of the above reasons, the improvement in the photoelectrochemical hydrogen production performance of the CdS-sensitized ZnO NRA after being hydrothermally grown twice can be attributed to the comparatively long ZnO nanorods, the

CdS nanoparticles with high crystallinity and large size, the single and compact layer, as well as the even distribution of CdS onto the ZnO nanorod surface.

4. CONCLUSIONS

ZnO NRA with comparatively long nanorods was successfully prepared on a Ti substrate by applying a hydrothermal method twice. CdS nanoparticles with a high crystallinity and diameters of 50 nm were galvanostatically electrodeposited as a compact and single layer onto the ZnO nanorod surface. Longer ZnO nanorods could provide more deposition sites for CdS nanoparticles. CdS-sensitized ZnO NRA could efficiently promote photogenerated electron mobility and increase the intensity of the interfacial electric field, thus exhibiting an efficient photoelectrochemical hydrogen production capacity from water reduction. The CdS-sensitized ZnO NRA after being hydrothermally grown twice with the second growth time of 6 h possessed the best photoelectrochemical performance. Under visible light, the photogenerated current density of this array at a 0 V bias potential is 15.8 $mA{\cdot}cm^{-2}$, 66.7% of that under white light. The IPCE is larger than 50% under the illumination of 380−520 nm light, indicating an extremely high visible light photoelectrochemical hydrogen production capacity from water reduction. In terms of photogenerated current density, the contribution from visible light is significantly higher than that from UV light. The CdS-sensitized ZnO NRA, prepared by conducting a hydrothermal growth method twice and by subsequently applying a galvanostatic electrodeposition method, exhibits a potential application in photoelectrochemical hydrogen production from water reduction under sunlight.

AUTHOR INFORMATION

Corresponding Author

*E-mail: zychen@qdio.ac.cn. Tel.: +86 532 8289 8731. Fax: +86 532 8288 0498.

Notes

The authors declare no competing financial interest.

ACKNOWLEDGMENTS

This work was financially supported by the Hundreds-Talent Program of the Chinese Academy of Sciences (Y02616101L).

REFERENCES

(1) Maeda, K.; Takata, T.; Hara, M.; Saito, N.; Inoue, Y.; Kobayashi, H.; Komen, K. *J. Am. Chem. Soc.* **2005**, *127*, 8286−8287.
(2) Wolcott, A.; Smith, W. A.; Kuykendall, T. A.; Zhao, Y. P.; Zhang, J. Z. *Adv. Fun. Mater.* **2009**, *19*, 1849−1856.
(3) Kudo, A.; Miseki, Y. *Chem. Soc. Rev.* **2009**, *38*, 253−278.
(4) Maeda, K.; Komen, K. *Chem. Mater.* **2010**, *22*, 612−623.
(5) Pauporte, T.; Rathouskv, J. *J. Phys. Chem. C* **2007**, *111*, 7639−7644.
(6) Hariharan, C. *Appl. Catal. A: Gen.* **2006**, *304*, 55−61.
(7) Dutta, B. K.; Chakrabarti, S. *J. Hazardous Mater.* **2004**, *112*, 269−278.
(8) Georgekutty, R.; Seery, M. K.; Pillai, S. C. *J. Phys. Chem. C* **2008**, *112*, 13563−13570.
(9) Law, M.; Greene, L. E.; Johnson, J. C.; Saykally, R.; Yang, P. *Nat. Mater.* **2005**, *4*, 455−459.
(10) Rensmo, H.; Keis, K.; Lindstrom, H.; Sodergren, S.; Solbrand, A.; Hagfeldt, A.; Lindquist, S. E. *J. Phys. Chem. B* **1997**, *101*, 2598−2601.
(11) Zhang, Q.; Dandeneau, C. S.; Zhou, X. Y.; Cao, G. Z. *Adv. Mater.* **2009**, *21*, 4087−4108.
(12) Rani, S.; Suri, P.; Shishodia, P. K.; Mehra, R. M. *Solar Energy Mater. Solar Cell* **2008**, *92*, 1639−1645.
(13) Seager, C. H.; Warren, W. L.; Tallant, D. R.; Voigt, J. A. *Appl. Phys. Lett.* **1996**, *68*, 403−405.
(14) Warren, W. L.; Seager, C. H.; Tallant, D. R.; Voigt, J. A.; Gnade, B. E. *Appl. Phys. Lett.* **1996**, *79*, 7983−7990.
(15) Li, Q. H.; Chen, Y. J.; Wang, T. H.; He, X. L.; Li, J. P.; Lin, C. L. *Appl. Phys. Lett.* **2004**, *84*, 3654−3656.
(16) Xu, J.; Pan, Q.; Shun, Y.; Tian, Z. *Sens. Actuators, B* **2000**, *66*, 277−279.
(17) Pan, H.; Misra, N.; Ko, S. H.; Grigoropoulos, C. P.; Miller, N.; Haller, E. E.; Dubon, O. *Appl. Phys. A: Mater. Sci. Process.* **2009**, *94*, 111−115.
(18) Sun, W. T.; Yu, Y.; Pan, H. Y.; Gao, X. F.; Chen, Q.; Peng, L. M. *J. Am. Chem. Soc.* **2008**, *130*, 1124−1125.
(19) Banerjee, S.; Mohapatra, S. K.; Das, P. P.; Misra, M. *Chem. Mater.* **2008**, *20*, 6784−6791.
(20) Gao, X. F.; Sun, W. T.; Hu, Z. D.; Ai, G.; Zhang, Y. L.; Feng, S.; Li, F.; Peng, L. M. *J. Phys. Chem. C* **2009**, *113*, 20481−20485.
(21) Wender, H.; Feil, A. F.; Diaz, L. B.; Ribeiro, C. S.; Machado, G. J.; Migowski, P.; Weibel, D. E.; Dupont, J.; Teixeira, S. R. *ACS Appl. Mater. Inter.* **2011**, *3*, 1359−1365.
(22) Qi, X.; She, G.; Liu, Y.; Mu, L.; Mu, L.; Shi, W. *Chem. Commun.* **2012**, *48*, 242−244.
(23) Wang, H.; Bai, Y.; Zhang, H.; Zhang, Z.; Li, J.; Guo, L. *J. Phys. Chem. C* **2010**, *114*, 16451−16455.
(24) Yang, S.; Nair, A. S.; Jose, R.; Ramakrishna, S. *Energy Environ. Sci.* **2010**, *3*, 2010−2014.
(25) Gao, T.; Li, Q.; Wang, T. *Chem. Mater.* **2005**, *17* (4), 887−892.
(26) Lee, W.; Min, K. S.; Dhas, V.; Ogale, S. B.; Han, S. H. *Electrochem. Commun.* **2009**, *11*, 103−106.
(27) Tang, Y.; Hua, X.; Chen, M.; Luo, L.; Li, B.; Zhang, L. *Electrochim. Acta* **2009**, *54*, 2742−2747.
(28) Seol, M.; Kim, H.; Kim, W.; Yong, K. *Electrochem. Commun.* **2010**, *12*, 1416−1418.
(29) Wang, G.; Yang, X.; Qian, F.; Zhang, J. Z.; Li, Y. *Nano Lett.* **2010**, *10*, 1088−1092.
(30) Chuangchote, S.; Jitputti, J.; Sagawa, T.; Yoshikawa, S. *ACS Appl. Mater. Interfaces* **2009**, *1*, 1140−1143.
(31) Emin, S.; Fanetti, M.; Abdi, F. F.; Lisjak, D.; Valant, M.; Krol, V. D. R.; Dam, B. *ACS Appl. Mater. Interfaces* **2013**, *5*, 1113−1121.
(32) Xu, F.; Dai, M.; Lu, Y.; Sun, L. *J. Phys. Chem. C* **2010**, *114*, 2776−2782.
(33) Ye, M.; Gong, J.; Lai, Y.; Lin, C.; Lin, Z. *J. Am. Chem. Soc.* **2012**, *134*, 15720−15723.
(34) Paulose, M.; Shankar, K.; Yoriya, S.; Prakasam, H. E.; Varghese, O. K.; Mor, G. K.; Latempa, T. A.; Fitzgerald, A.; Grimes, C. A *J. Phys. Chem. B* **2006**, *110*, 16179−16184.
(35) Li, G.; Zhang, D.; Yu, J. C. *Chem. Mater.* **2008**, *20*, 3983−3992.
(36) Greene, L. E.; Law, M.; Tan, D. H.; Montano, M.; Goldberger, J.; Somorjai, G.; Yang, P. *Nano Lett.* **2005**, *5*, 1231−1236.